



# CHORUS

This is the accepted manuscript made available via CHORUS. The article has been published as:

## Interlayer Electron-Hole Friction in Tunable Twisted Bilayer Graphene Semimetal

D. A. Bandurin, A. Principi, I. Y. Phinney, T. Taniguchi, K. Watanabe, and P. Jarillo-Herrero  
Phys. Rev. Lett. **129**, 206802 — Published 10 November 2022

DOI: [10.1103/PhysRevLett.129.206802](https://doi.org/10.1103/PhysRevLett.129.206802)

# Interlayer electron-hole friction in tunable twisted bilayer graphene semimetal

D.A. Bandurin,<sup>1</sup> A. Principi,<sup>2</sup> I.Y. Phinney,<sup>3</sup> T. Taniguchi,<sup>4</sup> K. Watanabe,<sup>5</sup> and P. Jarillo-Herrero<sup>3</sup>

<sup>1</sup>*Department of Materials Science and Engineering,  
National University of Singapore, 117575 Singapore*

<sup>2</sup>*School of Physics and Astronomy, University of Manchester, Manchester M13 9PL, United Kingdom*

<sup>3</sup>*Massachusetts Institute of Technology, Cambridge, MA 02139, USA*

<sup>4</sup>*International Center for Materials Nanoarchitectonics,  
National Institute of Material Science, Tsukuba 305-0044, Japan*

<sup>5</sup>*Research Center for Functional Materials, National Institute of Material Science, Tsukuba 305-0044, Japan*

Charge-neutral conducting systems represent a class of materials with unusual properties governed by electron-hole (e-h) interactions. Depending on the quasiparticles statistics, band structure, and device geometry these semimetallic phases of matter can feature unconventional responses to external fields that often defy simple interpretations in terms of single-particle physics. Here we show that small-angle twisted bilayer graphene (SA-TBG) offers a highly-tunable system in which to explore interactions-limited electron conduction. By employing a dual-gated device architecture we tune our devices from a non-degenerate charge-neutral Dirac fluid to a compensated two-component e-h Fermi liquid where spatially separated electrons and holes experience strong mutual friction. This friction is revealed through the  $T^2$  resistivity that accurately follows the e-h drag theory we develop. Our results provide a textbook illustration of a smooth transition between different interaction-limited transport regimes and clarify the conduction mechanisms in charge-neutral SA-TBG.

Low-dimensional electron-hole (e-h) systems have recently emerged as an important platform in which to explore many-body quantum phenomena. In such systems, strong Coulomb interaction among electrons and holes can give rise to a plethora of exotic quantum phases whose inventory encompasses superfluids<sup>1,2</sup>, correlated density wave states<sup>3,4</sup>, excitonic insulators<sup>5,6</sup>, and Wigner crystals<sup>4,7</sup>, to name a few. Particularly interesting interacting e-h mixtures are hosted by graphene and its bilayer. Graphene-based devices enabled the discovery of novel non-trivial effects governed by e-h interactions: from the Wiedemann-Franz law violation<sup>8</sup> and the anomalous Coulomb drag<sup>9-14</sup> to the quantum critical conductivity<sup>15-17</sup> and giant thermal diffusivity<sup>18</sup>. Central in these effects is the dominance of momentum-conserving e-h collisions over other momentum-relaxing scattering processes brought upon by graphene's weak electron-phonon coupling and low disorder<sup>19</sup>. As a result, the behavior of graphene's e-h plasma at elevated temperatures  $T$ , often referred to as Dirac fluid, resembles that of interacting relativistic fluids governed by the laws of (relativistic) hydrodynamics<sup>8,19-22</sup>. Since hydrodynamics offers a natural framework by which to probe the long-wavelength behavior of strongly-interacting fluids, experiments on model platforms, such as graphene, can give insights for observations in more exotic quantum phases of matter<sup>23,24</sup>, substantiating the interest in the field.

So far, the hydrodynamic behavior of interacting e-h plasmas in mono- and bilayer graphene (MLG and BLG respectively) was explored deep in the non-degenerate limit ( $E_F \ll k_B T$ , where  $E_F$  is the Fermi energy,  $k_B$  is the Boltzmann constant)<sup>8,18,25-27</sup>. The ambipolar hydrodynamics in the degenerate regime ( $E_F \gg k_B T$ ) as well as its genesis from the Boltzmann phase have at present remained inaccessible. This inaccessibility stems

from the fact that the conduction and valence band extrema in MLG and BLG coincide in momentum space and thus the e-h system can only be realized through the smearing of the charge neutrality point (NP); adding more carriers into the system converts the neutral Dirac fluid into a unipolar Fermi liquid (FL)<sup>19</sup>. In this work, we introduce biased SA-TBG as a convenient system in which to explore a smooth crossover between the Dirac fluid regime and the regime of degenerate e-h FL. In the latter case, we demonstrate that frequent momentum-conserving (yet velocity-relaxing) e-h collisions are the limiting factor for the SA-TBG conductivity.

We start by exploring the single-particle band structure of SA-TBG which is folded within a reduced Brillouin zone (BZ)<sup>31</sup> due to superlattice periodicity (Fig. 1a-b). At small energies, it resembles that of MLG but is characterized by a decreased Fermi velocity  $v_F$ . Like the BZ of MLG, the reduced BZ of SA-TBG is hexagonal and comprises two minivalleys located at the  $k_m$  and  $k'_m$  high symmetry points. These coincide with the  $K$  points of the two decoupled graphene sheets<sup>31</sup>. A prominent feature of the SA-TBG is that, away from the magic angle ( $\theta > 1.1^\circ$ ), one can selectively populate its minivalleys with charge carriers of opposite types using a perpendicular displacement field,  $D$ , (Fig. 1b)<sup>3,32-36</sup>. Electrostatic calculations<sup>33</sup> for  $D = 1$  V/nm, reveal that such a strong  $D$ , readily achievable in experiments, can result in the formation of relatively large electron and hole Fermi surfaces in the  $k_m$  and  $k'_m$  minivalleys, respectively. Quantitatively, in each minivalley, the Fermi temperature,  $T_F$ , exceeds room  $T$ , as in normal FLs (Fig. 1c dashed line). On the contrary, charge-neutral SA-TBG at  $D = 0$  is half-filled up to the Dirac point where the Fermi surfaces shrink to two points and where the Dirac fluid emerges at elevated  $T$ <sup>8,19</sup>. This tunability enables the exploration of e-h plasma at the crossover between the Dirac fluid

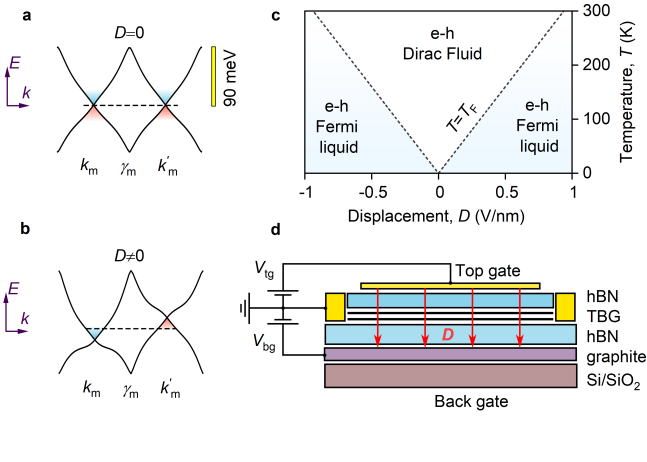


FIG. 1. **Biased SA-TBG.** **a-b**, Single-particle band structure for SA-TBG<sup>28,29</sup>. At low-energies, two Dirac cones are formed in the vicinity of the  $k_m$  and  $k'_m$  points (a); when  $D \neq 0$ , the cones are shifted with respect to each other (b). The horizontal dashed lines represent the Fermi level in the neutral SA-TBG. **c**, Phase diagram for the charge-neutral e-h mixture in SA-TBG mapped onto a  $T - D$  plane. Dashed lines: the dependence of  $T_F$  in each minivalley on  $D$  for  $n = 0$ . **d**, Schematic of the dual-gated encapsulated SA-TBG device.

and FL regimes in standard transport experiments as we schematically illustrate on the  $D - T$  diagram in Fig 1c.

To probe such a crossover, we fabricated a dual-gated multi-terminal Hall bar made out of  $\theta \approx 1.65^\circ$  SA-TBG encapsulated between two relatively thin ( $< 100$  nm thick) slabs of hexagonal boron nitride (hBN). At this angle, the SA-TBG is characterized by enhanced interaction strength and a reduced  $v_F$ , but is far enough from the magic angle ( $1.1^\circ$ ) that it allows for appreciable interlayer polarization<sup>3,34</sup>. The device was produced by a combination of tear-and-stack<sup>37-40</sup> and hot release<sup>41</sup> methods, and had a width of  $2 \mu\text{m}$  (Inset of Fig. 2b) Supplemental Material<sup>42</sup>). The dual-gated configuration (Fig. 1d) allowed us to control the interlayer displacement  $D/\epsilon_0 = (C_{\text{bg}}V_{\text{bg}} - C_{\text{tg}}V_{\text{tg}})/2$ , and the total externally-induced carrier density,  $n = (C_{\text{bg}}V_{\text{bg}} + C_{\text{tg}}V_{\text{tg}})/e$ , where  $C_{\text{tg,bg}}$  are the top and bottom gate capacitance per unit area,  $\epsilon_0$  is the dielectric permittivity of vacuum, and  $e$  is the electron charge.

Figure 2a shows an example of the longitudinal resistivity,  $\rho_{xx}$ , dependence on  $V_{\text{bg}}$  and  $V_{\text{tg}}$  in a form of 2D map, measured in our SA-TBG and reveals its characteristic behavior. Namely, the map consists of three diagonal lines: central - that denotes the global neutrality and two side diagonals, labeled as BI, that reflect the full filling of the first miniband where the single-particle band insulator emerges<sup>38,39,43</sup>. The BI lines allow for an accurate determination of the twist angle<sup>38,39,43</sup>. Below we will only focus on the region in the vicinity of the global neutrality and away from the BI and van Hove singularities.

Figure 2b shows the  $\rho_{xx}(n)$  dependence of our SA-TBG device measured at  $D = 0$  and  $T = 4.2$  K (the

curve is measured along the blue trace in the map from Fig. 2a). At  $D = 0$ ,  $\rho_{xx}(n)$  exhibits a sharp peak and reaches  $2.7 \text{ k}\Omega$  at  $n = 0$ , a standard behavior for SA-TBG devices. The peak width is only  $\delta n \simeq \times 10^{10} \text{ cm}^{-2}$  that indicates low charge inhomogeneity provided by the graphite gate<sup>44</sup>. Upon doping,  $\rho_{xx}(n)$  rapidly decreases and already at  $10^{12} \text{ cm}^{-2}$  drops to  $30 \Omega$  which translates to the  $1.7 \mu\text{m}$  mean free path, obtained from the standard Drude model. At liquid helium  $T$ , we also observed negative transfer resistance measured in the bend geometry ( Supplemental Material<sup>42</sup>), an indicative of the micrometre-scale ballistic transport<sup>45,46</sup>. These observations highlight an exceptional quality of our encapsulated SA-TBG device critical for further exploration of interaction-dominated transport at elevated  $T$ .

With the application of  $D$ , the transport properties of neutral SA-TBG change drastically (Fig. 2b, red curve).  $\rho_{xx}$  at the NP drops by more than an order of magnitude and becomes comparable to that of doped SA-TBG (cf.  $\rho_{xx}$  at  $10^{12} \text{ cm}^{-2}$ ). This qualitative behavior remains unchanged upon increasing  $T$  (Fig. 2c). Namely, at  $T = 20$  K the NP resistivities measured at zero and finite  $D$  differ by more than an order of magnitude. The drop of  $\rho_{xx}$  with increasing  $D$  signals parallel conduction of two minivalleys when each of them is doped away from their NPs.

Figures 3a-b shows  $\rho_{xx}(n)$  dependencies for varying  $T$  for the case of zero (a) and finite (b)  $D$  respectively. Away from the NP ( $n = 0$ ),  $\rho_{xx}$  grows with increasing  $T$  for both  $D$  values, indicating characteristic behavior of doped graphene sheets. On the contrary, at the NP,  $\rho_{xx}$  exhibits a very different behavior for the two cases. Namely, at  $D = 0$ ,  $\rho_{xx}$  drops rapidly when  $T$  is raised from 4.2 to 40 K (inset of Fig. 3a), whereas at  $D = 0.7$  V/nm,  $\rho_{xx}$  shows a clear metallic trend: the resistivity increases with increasing  $T$  (inset of Fig. 3b).

It is now instructive to normalize all measured  $\rho_{xx}(T)$  dependencies to their lowest  $T$  value in order to compare the functional forms of the  $T$ -dependencies in different cases. At  $T = 40$  K, the zero- $D$  resistivity of the SA-TBG device is less than a half of its 4.2 K value; further increase of  $T$  leads to a very slow ascending trend of  $\rho_{xx}(T)$ . At the same  $T$  and  $D = 0.7$  V/nm,  $\rho_{xx}$  experiences more than two times increase and keeps growing with increasing  $T$  following approximately an  $a + bT^2$  dependence, where  $a$  and  $b$  are constants (dashed black line in the inset of Fig. 3b). To compare, we have also measured the resistivity of a BLG device of comparable quality as a function of  $n$  and  $T$  (Fig. 3c). At the NP,  $\rho_{xx}$  is practically unaffected by the  $T$  variation (Fig. 3c) over the entire range of  $T$  in our experiments.

The above observations clearly point to the difference in the conductivity mechanisms of these three bilayer systems at their NPs. The weak insulating behavior of charge-neutral SA-TBG at zero  $D$  resembles that of MLG: the resistivity drops as a result of the thermal activation of electrons and holes<sup>8</sup>. A further increase of  $T$  leads to the enhanced scattering between electron

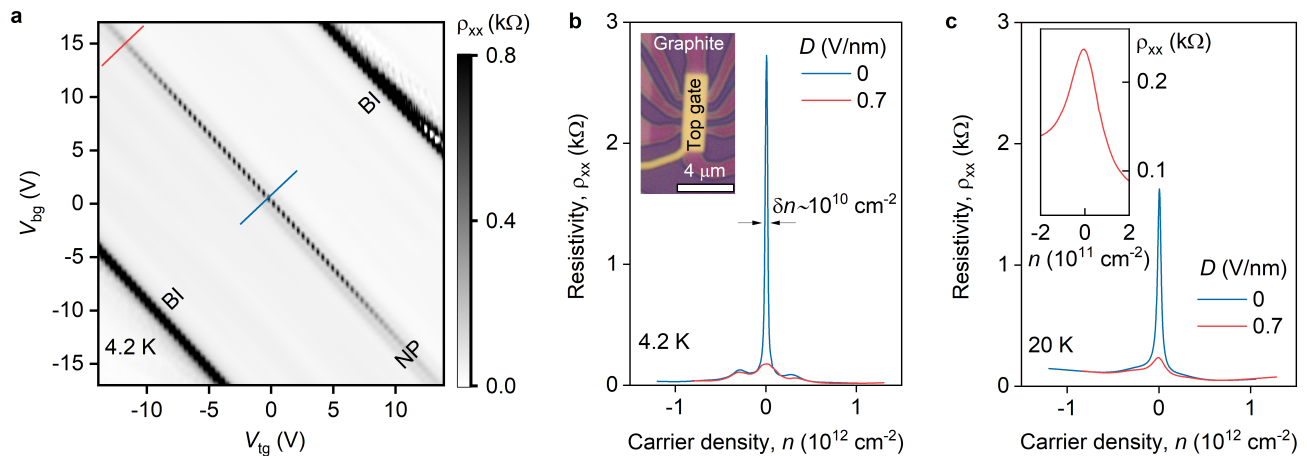


FIG. 2. **Effect of displacement on the transport properties of the SA-TBG.** **a**,  $\rho_{xx}$  as a function of  $V_{bg}$  and  $V_{tg}$  measured in the  $1.65^\circ$  SA-TBG device. Blue and red lines correspond to the  $(V_{tg}, V_{bg})$  points where  $D = 0$  and  $D = 0.7$  V/nm respectively. **b**,  $\rho_{xx}(n)$  traces for  $D = 0$  and  $D = 0.7$  V/nm measured at  $T = 4.2$  K. Inset: Optical photograph of an encapsulated SA-TBG device. We attribute low- $T$  bulges in the resistivity at  $|n| \simeq 10^{11}$   $\text{cm}^{-2}$  to the manifestation of composite super-moiré lattices with a very long wavelength that could form due to unintentional and coarse alignment of graphene sheets with both boron nitride flakes<sup>30</sup>. **c**, Same as (b) but for  $T = 20$  K. Inset: zoomed-in region of the NP vicinity for  $D = 0.7$  V/nm.

184 and hole non-degenerate sub-systems hosted by SA-TBG<sup>215</sup>  
 185 leading to an increase of the resistivity. In contrast,<sup>216</sup>  
 186 the flat  $T$ -dependence of the BLG has been recently<sup>217</sup>  
 187 attributed to the perfect balance between the amount<sup>218</sup>  
 188 of thermally activated e-h pairs facilitating conductiv-<sup>219</sup>  
 189 ity, and the e-h scattering that impedes the electrical<sup>220</sup>  
 190 current<sup>22,26,47</sup>. The peculiar  $T^2$  growth of the resistivity<sup>221</sup>  
 191 in compensated SA-TBG at finite  $D$  has not been ob-<sup>222</sup>  
 192 served previously. Below we show that this effect stems<sup>223</sup>  
 193 from the e-h friction<sup>48,49</sup> in this degenerate ambipolar<sup>224</sup>  
 194 system. <sup>225</sup>

195 To demonstrate this, we solve the steady-state Boltz-<sup>226</sup>  
 196 mann equation for e-h hole mixture in SA-TBG; the de-<sup>227</sup>  
 197 tails are given in Supplemental Material<sup>42</sup>. In the limit of<sup>228</sup>  
 198 temperatures much smaller than  $T_F$ , the resistivity due<sup>229</sup>  
 199 to e-h scattering reads <sup>230</sup>

$$\rho_D \simeq \frac{8\pi\alpha_{ee}^2 g(\bar{q}_{TF})}{3ne^2 v_F^2 \hbar} (k_B T)^2. \quad (1) \quad 231$$

200 where  $n$  is the particle density in each minivalley,<sup>234</sup>  
 201  $g(\bar{q}_{TF}) = 3(\bar{q}_{TF} - 1) + (4 - 3\bar{q}_{TF}^2)\text{arccoth}(1 + \bar{q}_{TF})$  and<sup>235</sup>  
 202  $\bar{q}_{TF} = N_f \alpha_{ee}$  is the Thomas-Fermi screening wavevec-<sup>236</sup>  
 203 tor in units of the Fermi wavevector. Here,  $\alpha_{ee} =$ <sup>237</sup>  
 204  $e^2 / (2\pi\epsilon_0(\epsilon_r + 1)\hbar v_F)$  is the effective fine-structure con-<sup>238</sup>  
 205 stant of Dirac fermions,  $\epsilon_r$  is a dielectric constant ac-<sup>239</sup>  
 206 counting for screening due to far bands and external di-<sup>240</sup>  
 207 electrics,  $N_f$  is the number of flavors, and  $\hbar$  is the re-<sup>241</sup>  
 208 duced Planck constant. Hereafter we set  $\epsilon_r = 3.9$ , as<sup>242</sup>  
 209 for graphene deposited on hBN. The total resistivity is<sup>243</sup>  
 210 then  $\rho = \rho_0 + \rho_D$ , where  $\rho_0$  is the zero-temperature resis-<sup>244</sup>  
 211 tivity due to momentum-non-conserving scattering pro-<sup>245</sup>  
 212 cesses. We also note that, as the minivalleys are pre-<sup>246</sup>  
 213 dominantly formed from the energy bands of different<sup>247</sup>  
 214 graphene sheets, electrons and holes reside in the up-<sup>248</sup>

per or lower graphene layers depending on the  $D$  direc-  
 tion<sup>3,33,34</sup>, and thus  $\rho_D$  can be interpreted as the resistiv-  
 ity due to the interlayer e-h friction (See Supplemental  
 Material<sup>42</sup>).

In Fig. 3d we compare the results of our calculations  
 with  $\rho_{xx}(T)$  found experimentally. To this end, we  
 plot the experimentally found resistivity excess,  $\Delta\rho =$   
 $\rho_{xx}(T) - \rho_{xx}(4.2 \text{ K})$ , and theoretically obtained  $\rho_D(T)$ .  
 For the latter, we used an electrostatic model that ac-  
 counts for screening effects to calculate the Fermi en-  
 ergy in each minivalley<sup>33</sup>, as well as the experimentally  
 determined twist angle. Using that, for  $\theta = 1.65^\circ$ ,  
 $v_F \simeq 5 \times 10^5$  m/s (as determined from the continuum  
 model of SA-TBG<sup>28,29,31</sup>), for  $D = 0.7$  V/m we estimate  
 the carrier density  $n = 1.3 \times 10^{15}$   $\text{m}^{-2}$ . Experimental  
 data follows closely the expected  $\mathcal{B}T^2$  dependence with  
 $\mathcal{B} \simeq 0.062$   $\Omega/\text{K}^2$  with some tendency to sub-quadratic  
 dependence at higher  $T$  (inset of Fig. 3b).

Next, we analyze  $\rho_D(T)$  dependencies expected for  
 other  $\theta$ . We find that, at fixed carrier density, the resis-  
 tivity due to e-h scattering depends on  $\theta$  only through  
 its dependence on the electron Fermi velocity  $v_F$ . In the  
 inset of Fig. 3 we plot the ratio  $\mathcal{B}(v_F)/\mathcal{B}(v_F^g)$  for a carrier  
 density  $n = 4 \times 10^{14}$   $\text{m}^{-2}$  as a function of  $\theta$ . Here,  $v_F^g$   
 is the Fermi velocity of MLG, while  $\mathcal{B}(v_F)$  is defined from  
 $\rho_D = \mathcal{B}(v_F)T^2$ . At  $\theta > 3^\circ$  the e-h drag would result in a  
 10 times smaller prefactor of the  $T^2$ -resistivity.

It would be instructive to put our observations in the  
 context of electron transport in semimetals. Depending  
 on the material, seemingly alike semimetallic e-h systems  
 can display very different physical properties. For exam-  
 ple, in charge-neutral MLG, frequent collisions between  
 thermally activated electrons and holes impede electrical  
 currents while leaving thermal ones untouched, causing

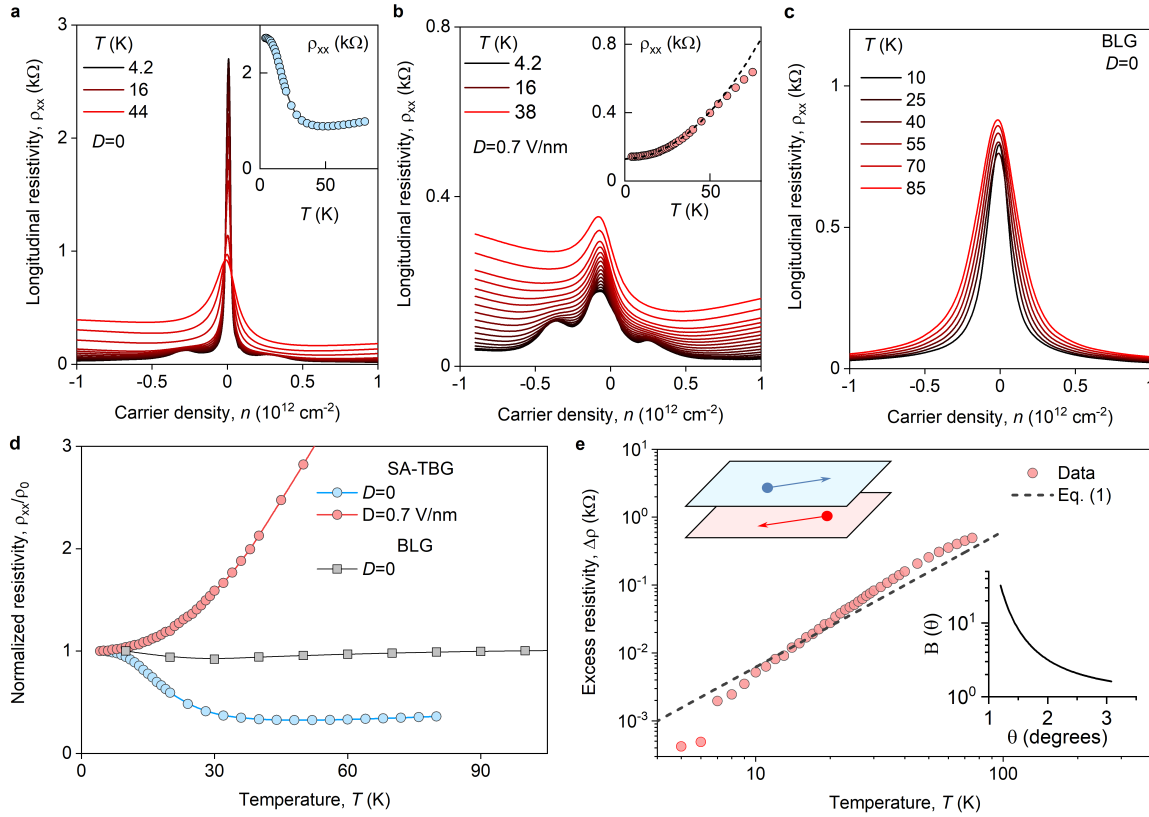


FIG. 3. **Temperature dependence of the SA-TBG resistivity** **a**,  $\rho_{xx}(n)$  for different  $T$  for the case of  $D = 0$ . Inset:  $\rho_{xx}(T)$  at the NP and  $D = 0$ . **b**, Same as (a) but for  $D = 0.7$  V/nm. Inset:  $\rho_{xx}(T)$  at the compensation point ( $n = 0$ ) and  $D = 0.7$  V/nm. Dashed line: guide for the eye that represents the  $a + bT^2$  dependence. The deviation from the  $T^2$  scaling can be attributed to the thermal smearing of the distribution function that leads to the exit of the SA-TBG e-h system from the degenerate state: at  $n = 1.3 \times 10^{11} \text{ cm}^{-2}$ , the Fermi temperature of the  $1.65^\circ$  SA-TBG is of the order of 220 K. **c**,  $\rho_{xx}(n)$  for BLG at  $D = 0$ . **d**, Resistivity as a function of  $T$  for the charge-neutral SA-TBG at  $D = 0$  (blue) and  $D = 0.7$  V/nm (red) and for BLG at  $D = 0$  (grey). The data is normalized to the lowest- $T$  value of  $\rho_{xx}(n)$ : 4.2 K for SA-TBG and 10 K for BLG. **e**,  $\Delta\rho = \rho_{xx}(T) - \rho_{xx}(4.2 \text{ K})$  as a function of  $T$  measured at  $D = 0.7$  V/nm and  $n = 0$  (symbols). Note,  $\Delta\rho(T)$  exhibits somewhat faster  $T$ -dependence at  $T < 15$  K. This apparent behavior is spurious and is related to the subtraction operation of the  $\rho_0 = \rho_{xx}(4.2 \text{ K})$  from the experimental dataset rather than  $\rho_{xx}$  at  $T \rightarrow 0$ . Solid line: theoretical dependence, eq. (1). Upper left inset: schematic illustration of the interlayer e-h friction in SA-TBG at finite  $D$ . Lower right inset: Prefactor  $\mathcal{B}$  as a function of twist angle,  $\theta$ .

249 a breakdown of the Wiedeman-Franz law. In this sys-267  
 250 tem the Lorentz ratio, i.e. the ratio between the ther-268  
 251 mal conductivity and its electrical counterpart, is found269  
 252 to be greatly enhanced<sup>8</sup>. On the contrary, in degen-270  
 253 erate compensated semimetals such as  $\text{WP}_2$  or  $\text{Sb}$  the271  
 254 Lorentz ratio has been found to be suppressed<sup>50</sup>. De-272  
 255 spite their semimetallic nature, which would imply viola-273  
 256 tions of the Wiedeman-Franz law akin to those observed274  
 257 in graphene<sup>51</sup>, the behavior of these materials closely re-275  
 258 sembles that of conventional unipolar systems<sup>52</sup>, where276  
 259 carriers of a single type transport both charge and heat.277  
 260 All these seemingly contradictory observations have stim-  
 261 ulated a debate over the effect of quasiparticle statistics,  
 262 band structure and many-body interactions on the ther-  
 263 mal and electrical properties of these charge-neutral ma-  
 264 terial platforms<sup>51,53,54</sup>. A definitive resolution of these  
 265 long lasting puzzles is made especially difficult by the  
 266 fact that completely different behaviors are observed in280

different systems and regimes, and therefore a thorough  
 comparison between them becomes challenging. The behav-  
 ior of SA-TBG observed in this work thus makes it  
 a highly-tunable platform for the exploration of different  
 semimetallic regimes on an equal footing, allowing for a  
 gradual transition between them. It would be further inter-  
 esting to explore transport and thermal properties of  
 e-h FLs in other polarizable layered systems with heavier  
 charge carriers such as twisted double bilayer graphene<sup>3</sup>  
 or twisted transition metal dichalcogenides<sup>6</sup> as well as to  
 probe collective modes in such e-h mixtures<sup>55-57</sup>.

\*Correspondence to: dab@nus.edu.sg,  
 alepr85@gmail.com and pjarillo@mit.edu.

## ACKNOWLEDGMENTS

This work was supported by AFOSR grant FA9550-21-1-0319 and the Gordon and Betty Moore Foundations EPiQS Initiative through Grant GBMF9463 to P.J.-H.. I.Y.P. acknowledges support from the MIT undergraduate research opportunities program and the Johnson and Johnson research scholars program. K.W. and T.T. acknowledge support from JSPS KAKENHI (Grant Numbers 19H05790, 20H00354 and 21H05233). A.P. acknowledges support from the European Commission under the EU Horizon 2020 MSCA-RISE-2019 programme (project 873028 HYDROTRONICS) and from the Leverhulme Trust under the grant RPG-2019-363. The authors thank Clement Collignon, Alexey Berdyugin and Dmitry Svintsov for productive discussions.

## DATA AVAILABILITY

The data reported in Figs. 23 can be found on Zenodo (<https://doi.org/10.5281/zenodo.7256407>). The other

data that support the findings of this study are available from the corresponding authors upon reasonable request.

## AUTHOR CONTRIBUTIONS

D.A.B. and A.P. conceived and designed the study. D.A.B. and I.Y.P. fabricated and measured the devices. T.T. and K.W. grew high-quality hBN crystals. A.P. developed the theory. P.J.H. supervised the project.

## COMPETING INTERESTS

The authors declare no competing interests.

- <sup>1</sup> J. P. Eisenstein and A. H. MacDonald, *Nature* **432**, 691 (2004).
- <sup>2</sup> A. Perali, D. Neilson, and A. R. Hamilton, *Phys. Rev. Lett.* **110**, 146803 (2013).
- <sup>3</sup> P. Rickhaus, F. K. de Vries, J. Zhu, E. Portoles, G. Zheng, M. Masseroni, A. Kurzman, T. Taniguchi, K. Watanabe, A. H. MacDonald, T. Ihn, and K. Ensslin, *Science* **373**, 1257 (2021).
- <sup>4</sup> M. Zarenia, D. Neilson, and F. M. Peeters, *Scientific Reports* **7**, 11510 (2017).
- <sup>5</sup> Y. Jia, P. Wang, C.-L. Chiu, Z. Song, G. Yu, B. Jäck, S. Lei, S. Klemen, F. A. Cevallos, M. Onyszczak, N. Fishchenko, X. Liu, G. Farahi, F. Xie, Y. Xu, K. Watanabe, T. Taniguchi, B. A. Bernevig, R. J. Cava, L. M. Schoop, A. Yazdani, and S. Wu, *Nature Physics* **18**, 87 (2022).
- <sup>6</sup> Z. Zhang, E. C. Regan, D. Wang, W. Zhao, S. Wang, M. Sayyad, K. Yumigeta, K. Watanabe, T. Taniguchi, S. Tongay, M. Crommie, A. Zettl, M. P. Zaletel, and F. Wang, *Nature Physics* **18**, 1214 (2022).
- <sup>7</sup> S. Rakhmanov, *Zhurnal Eksperimental'noj i Teoreticheskoy Fiziki* **75**, 160 (1978).
- <sup>8</sup> J. Crossno, J. K. Shi, K. Wang, X. Liu, A. Harzheim, A. Lucas, S. Sachdev, P. Kim, T. Taniguchi, K. Watanabe, T. A. Ohki, and K. C. Fong, *Science* **351**, 1058 (2016).
- <sup>9</sup> R. V. Gorbachev, A. K. Geim, M. I. Katsnelson, K. S. Novoselov, T. Tudorovskiy, I. V. Grigorieva, A. H. MacDonald, S. V. Morozov, K. Watanabe, T. Taniguchi, and L. A. Ponomarenko, *Nature Physics* **8**, 896 (2012).
- <sup>10</sup> J. I. A. Li, T. Taniguchi, K. Watanabe, J. Hone, A. Levchenko, and C. R. Dean, *Phys. Rev. Lett.* **117**, 046802 (2016).
- <sup>11</sup> J. C. W. Song, D. A. Abanin, and L. S. Levitov, *Nano Letters* **13**, 3631 (2013).
- <sup>12</sup> M. Titov, R. V. Gorbachev, B. N. Narozhny, T. Tudorovskiy, M. Schütt, P. M. Ostrovsky, I. V. Gornyi, A. D. Mirlin, M. I. Katsnelson, K. S. Novoselov, A. K. Geim, and L. A. Ponomarenko, *Phys. Rev. Lett.* **111**, 166601 (2013).
- <sup>13</sup> M. Schütt, P. M. Ostrovsky, M. Titov, I. V. Gornyi, B. N. Narozhny, and A. D. Mirlin, *Phys. Rev. Lett.* **110**, 026601 (2013).
- <sup>14</sup> J. C. W. Song and L. S. Levitov, *Phys. Rev. Lett.* **111**, 126601 (2013).
- <sup>15</sup> L. Fritz, J. Schmalian, M. Müller, and S. Sachdev, *Phys. Rev. B* **78**, 085416 (2008).
- <sup>16</sup> M. Müller, J. Schmalian, and L. Fritz, *Phys. Rev. Lett.* **103**, 025301 (2009).
- <sup>17</sup> P. Gallagher, C.-S. Yang, T. Lyu, F. Tian, R. Kou, H. Zhang, K. Watanabe, T. Taniguchi, and F. Wang, *Science* **364**, 158 (2019).
- <sup>18</sup> A. Block, A. Principi, N. C. H. Hesp, A. W. Cummings, M. Liebel, K. Watanabe, T. Taniguchi, S. Roche, F. H. L. Koppens, N. F. van Hulst, and K.-J. Tielrooij, *Nature Nanotechnology* **16**, 1195 (2021).
- <sup>19</sup> A. Lucas and K. C. Fong, *Journal of Physics: Condensed Matter* **30**, 053001 (2018).
- <sup>20</sup> D. Svintsov, V. Vyurkov, S. Yurchenko, T. Otsuji, and V. Ryzhii, *Journal of Applied Physics* **111**, 083715 (2012).
- <sup>21</sup> B. N. Narozhny, I. V. Gornyi, M. Titov, M. Schütt, and A. D. Mirlin, *Phys. Rev. B* **91**, 035414 (2015).
- <sup>22</sup> D. Y. H. Ho, I. Yudhistira, N. Chakraborty, and S. Adam, *Phys. Rev. B* **97**, 121404 (2018).
- <sup>23</sup> C. Cao, E. Elliott, J. Joseph, H. Wu, J. Petricka, T. Schfer, and J. E. Thomas, *Science* **331**, 58 (2011).
- <sup>24</sup> E. Shuryak, *Progress in Particle and Nuclear Physics* **53**, 273 (2004), heavy Ion Reaction from Nuclear to Quark Matter.
- <sup>25</sup> Y. Nam, D.-K. Ki, D. Soler-Delgado, and A. F. Morpurgo, *Nature Physics* **13**, 1207 (2017).

- 377 <sup>26</sup> C. Tan, D. Y. H. Ho, L. Wang, J. I. A. Li, I. Yudhistira,<sup>429</sup>  
378 D. A. Rhodes, T. Taniguchi, K. Watanabe, K. Shepard,<sup>430</sup>  
379 P. L. McEuen, C. R. Dean, S. Adam, and J. Hone, *Science*<sup>431</sup>  
380 [Advances](#) **8**, eabi8481 (2022).<sup>432</sup>
- 381 <sup>27</sup> A. I. Berdyugin, N. Xin, H. Gao, S. Slizovskiy, Z. Dong,<sup>433</sup>  
382 S. Bhattacharjee, P. Kumaravadivel, S. Xu, L. A. Ponomorenko,<sup>434</sup>  
383 M. Holwill, D. A. Bandurin, M. Kim, Y. Cao,<sup>435</sup>  
384 M. T. Greenaway, K. S. Novoselov, I. V. Grigorieva,<sup>436</sup>  
385 K. Watanabe, T. Taniguchi, V. I. Fal'ko, L. S. Levitov,<sup>437</sup>  
386 R. K. Kumar, and A. K. Geim, *Science* **375**, 430 (2022).<sup>438</sup>
- 387 <sup>28</sup> S. Fang, S. Carr, Z. Zhu, D. Massatt, and E. Kaxiras,<sup>439</sup>  
388 "Angle-dependent *ab initio* low-energy hamiltonians for a<sup>440</sup>  
389 relaxed twisted bilayer graphene heterostructure," (2019),<sup>441</sup>  
390 [arXiv:1908.00058 \[cond-mat.mes-hall\]](#).<sup>442</sup>
- 391 <sup>29</sup> S. Carr, S. Fang, Z. Zhu, and E. Kaxiras, *Phys. Rev.*<sup>443</sup>  
392 [Research](#) **1**, 013001 (2019).<sup>444</sup>
- 393 <sup>30</sup> Z. Wang, Y. B. Wang, J. Yin, E. Tóvári, Y. Yang, L. Lin,<sup>445</sup>  
394 M. Holwill, J. Birkbeck, D. J. Perello, S. Xu, J. Zultak,<sup>446</sup>  
395 R. V. Gorbachev, A. V. Kretinin, T. Taniguchi, K. Watanabe,<sup>447</sup>  
396 S. V. Morozov, M. Andelković, S. P. Milovanović,<sup>448</sup>  
397 L. Covaci, F. M. Peeters, A. Mishchenko, A. K. Geim,<sup>449</sup>  
398 K. S. Novoselov, V. I. Fal'ko, A. Knothe, and C. Woods,<sup>450</sup>  
399 *Science Advances* **5**, eaay8897 (2022).<sup>451</sup>
- 400 <sup>31</sup> R. Bistritzer and A. H. MacDonald, *Proceedings of the*<sup>452</sup>  
401 *National Academy of Science* **108**, 12233 (2011).<sup>453</sup>
- 402 <sup>32</sup> J. D. Sanchez-Yamagishi, T. Taychatanapat, K. Watanabe,<sup>454</sup>  
403 T. Taniguchi, A. Yacoby, and P. Jarillo-Herrero,<sup>455</sup>  
404 *Phys. Rev. Lett.* **108**, 076601 (2012).<sup>456</sup>
- 405 <sup>33</sup> S. Slizovskiy, A. Garcia-Ruiz, A. I. Berdyugin, N. Xin,<sup>457</sup>  
406 T. Taniguchi, K. Watanabe, A. K. Geim, N. D. Drummond,<sup>458</sup>  
407 and V. I. Fal'ko, *Nano Letters* **21**, 6678 (2021).<sup>459</sup>
- 408 <sup>34</sup> F. K. de Vries, J. Zhu, E. Portolés, G. Zheng,<sup>460</sup>  
409 M. Masseroni, A. Kurzmamann, T. Taniguchi, K. Watanabe,<sup>461</sup>  
410 A. H. MacDonald, K. Ensslin, T. Ihn, and P. Rickhaus,<sup>462</sup>  
411 *Phys. Rev. Lett.* **125**, 176801 (2020).<sup>463</sup>
- 412 <sup>35</sup> A. I. Berdyugin, B. Tsim, P. Kumaravadivel, S. G. Xu,<sup>464</sup>  
413 A. Ceferino, A. Knothe, R. K. Kumar, T. Taniguchi,<sup>465</sup>  
414 K. Watanabe, A. K. Geim, I. V. Grigorieva, and V. I.<sup>466</sup>  
415 Fal'ko, *Science Advances* **6**, eaay7838 (2020).<sup>467</sup>
- 416 <sup>36</sup> I. Y. Phinney, D. A. Bandurin, C. Collignon, I. A.<sup>468</sup>  
417 Dmitriev, T. Taniguchi, K. Watanabe, and P. Jarillo-Herrero,<sup>469</sup>  
418 *Phys. Rev. Lett.* **127**, 056802 (2021).<sup>470</sup>
- 419 <sup>37</sup> K. Kim, M. Yankowitz, B. Fallahazad, S. Kang, H. C. P.<sup>471</sup>  
420 Movva, S. Huang, S. Larentis, C. M. Corbet, T. Taniguchi,<sup>472</sup>  
421 K. Watanabe, S. K. Banerjee, B. J. LeRoy, and E. Tutuc,<sup>473</sup>  
422 *Nano Letters* **16**, 1989 (2016).<sup>474</sup>
- 423 <sup>38</sup> K. Kim, A. DaSilva, S. Huang, B. Fallahazad, S. Larentis,<sup>475</sup>  
424 T. Taniguchi, K. Watanabe, B. J. LeRoy, A. H. MacDonald,<sup>476</sup>  
425 and E. Tutuc, *Proceedings of the National Academy*  
426 *of Sciences* **114**, 3364 (2017).<sup>477</sup>
- 427 <sup>39</sup> Y. Cao, J. Y. Luo, V. Fatemi, S. Fang, J. D. Sanchez-  
428 Yamagishi, K. Watanabe, T. Taniguchi, E. Kaxiras, and  
P. Jarillo-Herrero, *Phys. Rev. Lett.* **117**, 116804 (2016).<sup>478</sup>
- 40 <sup>40</sup> J. M. Park, Y. Cao, K. Watanabe, T. Taniguchi, and  
P. Jarillo-Herrero, *Nature* **592**, 43 (2021).<sup>479</sup>
- 41 <sup>41</sup> D. G. Purdie, N. M. Pugno, T. Taniguchi, K. Watanabe,  
A. C. Ferrari, and A. Lombardo, *Nature Communications*  
**9**, 5387 (2018).<sup>480</sup>
- 42 <sup>42</sup> See Supplemental Material at  
<http://link.aps.org/supplemental/> for device fabrication  
details, signatures of ballistic transport, and theoretical  
calculations of the interaction-dominated resistivity in  
SA-TBG.<sup>481</sup>
- 43 <sup>43</sup> Y. Kim, P. Herlinger, P. Moon, M. Koshino, T. Taniguchi,  
K. Watanabe, and J. H. Smet, *Nano Letters* **16**, 5053  
(2016).<sup>482</sup>
- 44 <sup>44</sup> A. A. Zibrov, E. M. Spanton, H. Zhou, C. Kometter,  
T. Taniguchi, K. Watanabe, and A. F. Young, *Nature*  
*Physics* **14**, 930 (2018).<sup>483</sup>
- 45 <sup>45</sup> C. W. J. Beenakker and H. van Houten, *Phys. Rev. Lett.*  
**63**, 1857 (1989).<sup>484</sup>
- 46 <sup>46</sup> A. S. Mayorov, R. V. Gorbachev, S. V. Morozov, L. Britnell,  
R. Jalil, L. A. Ponomorenko, P. Blake, K. S.  
Novoselov, K. Watanabe, T. Taniguchi, and A. K. Geim,  
*Nano Letters* **11**, 2396 (2011).<sup>485</sup>
- 47 <sup>47</sup> G. Wagner, D. X. Nguyen, and S. H. Simon, *Phys. Rev.*  
*Lett.* **124**, 026601 (2020).<sup>486</sup>
- 48 <sup>48</sup> Z. D. Kvon, E. B. Olshanetsky, D. A. Kozlov, E. Novik,  
N. N. Mikhailov, and S. A. Dvoretzky, *Low Temperature*  
*Physics* **37**, 202 (2011).<sup>487</sup>
- 49 <sup>49</sup> V. L. Müller, Y. Yan, O. Kashuba, B. Trauzettel, M. Abdelghany,  
J. Kleinlein, W. Beugeling, H. Buhmann, and  
L. W. Molenkamp, *Nano Letters* **0**, null (0).<sup>488</sup>
- 50 <sup>50</sup> J. Gooth, F. Menges, N. Kumar, V. Süß, C. Shekhar,  
Y. Sun, U. Drechsler, R. Zierold, C. Felser, and B. Gotsmann,  
*Nature Communications* **9**, 4093 (2018).<sup>489</sup>
- 51 <sup>51</sup> M. Zarenia, A. Principi, and G. Vignale, *Phys. Rev. B*  
**102**, 214304 (2020).<sup>490</sup>
- 52 <sup>52</sup> A. Principi and G. Vignale, *Phys. Rev. Lett.* **115**, 056603  
(2015).<sup>491</sup>
- 53 <sup>53</sup> S. Li and D. L. Maslov, *Phys. Rev. B* **98**, 245134 (2018).<sup>492</sup>
- 54 <sup>54</sup> P. S. Alekseev, A. P. Dmitriev, I. V. Gornyi, V. Y. Kachorovskii,  
B. N. Narozhny, M. Schütt, and M. Titov,  
*Phys. Rev. Lett.* **114**, 156601 (2015).<sup>493</sup>
- 55 <sup>55</sup> V. Andreeva, D. A. Bandurin, M. Luskin, and D. Margetis,  
*Phys. Rev. B* **102**, 205411 (2020).<sup>494</sup>
- 56 <sup>56</sup> A. Principi, D. Bandurin, H. Rostami, and M. Polini,  
*Phys. Rev. B* **99**, 075410 (2019).<sup>495</sup>
- 57 <sup>57</sup> Z. Sun, D. N. Basov, and M. M. Fogler, *Proceedings of*  
*the National Academy of Sciences* **115**, 3285 (2018).<sup>496</sup>